33RD CONGRESS
OF THE INTERNATIONAL COUNCIL
OF THE AERONAUTICAL SCIENCES
STOCKHOLM, SWEDEN, 4-9 SEPTEMBER, 2022

ICAS 2022 SWEDEN

ANALYSIS AND SIZING OF GREEN PROPULSION SYSTEM FOR A SUBORBITAL AIRCRAFT

Martina Bruno[1], Riccardo Cambertoni[2], Alberto Pellegrino[3], Pierluigi Petrachi[4] & Cristina Spampinato[5]

[1]Polytechnic of Turin

Abstract

The following paper deals with achieving a sustainable propulsion system for the vehicle SALTO I [16], that is the vehicle conceived by the PoliTOrbital team, designed for manned suborbital flights. This work will follow the high level requirements given by the Aerospace Challenge [15]. The propulsion system will consist of two air breathing engines, useful for the first take-off phase and a rocket engine, which will be switched on at 12 km. Then the aircraft will carry out 4 minutes of weightlessness flight with the engines off at the maximum altitude and subsequently the air breathing engines will be re-started for the descent phase. The main aim is to reach a compromise between performances and environmental sustainability.

1. General Introduction

A suborbital flight is a flight beyond 100 km above sea level in which the vehicle does not reach the speed to escape Earth's gravity field. When a suborbital space vehicle of current design reaches its maximum altitude at the vertex of the parabola, the horizontal speed is almost zero. The public interest leads this industry to improve and develop projects on suborbital flights from private aerospace agencies. Different designs were proposed, such as Blue Origin's Blue Shepard, that is characterized by a liquid (LOX/LH_2) rocket engine, following the structure of common launchers or Virgin Galactic's SpaceShipTwo, which has instead the structural characteristics of an aeronautical vehicle. SALTO I follows the latter one, but the take-off is made by its own air breathing engines.

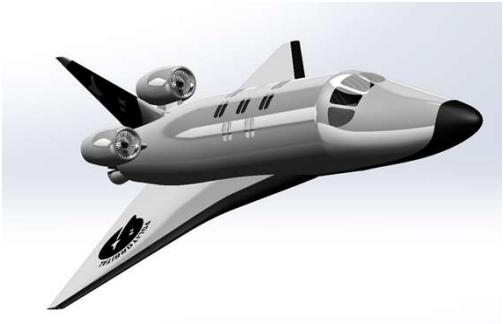

Figure 1 - SALTO I

2. Rocket Engine

In order to accurately select the optimal type of engine, all available alternatives were analyzed for the rocket propulsion system. Are here summarized some considerations about possible green fuels and oxidizers between liquid and solid [13]:

- Nitrous oxide N_2O [Liquid oxidizer]: N_2O is the only compound on binary nitrogen/oxygen that is considered "green" [8]. N_2O possesses good storable characteristics at room temperature, especially for long term retention since it does not have decomposition or boiling problems when compared to H_2O_2 or cryogenic LOX. This oxidizer has self-pressurizing properties, avoiding the need for additional helium pressurizing systems.
- Hydrogen Peroxide H_2O_2 [Liquid oxidizer]: it is not only a powerful liquid oxidizer when burning with an organic fuel but also clean burning. It is moreover leading rocket propellants for satellite and upper stage propulsion.
- LCH_4/LO_2 and LH_2/LO_2 [Liquid propeller]: These two cryogenic bi-propellants are the most used rocket fuels combination. Methane and hydrogen have a lower level of toxicity than the most common propellants, so they are of interest for a study of green propellants. Although LH_2/LO_2

is a high performance mixture, it has unfortunately low fuel density, which requires bulky and large fuel tanks.

- HTPB [Solid Fuel]: Research has been done in the literature for the various liquid oxidant/solid fuel combinations for hybrid engine structure, subsequently selecting the solution that uses Nitrous oxide N_2O as the liquid oxidant and HTPB as the solid fuel. It is the most common for a hybrid propellant, it has a relatively low environmental impact [1] and, above all, is already used by Virgin Galactic's SpaceShipTwo. An analysis was conducted on the combustion products of this mixture, obtaining results that confirm their low environmental impact.

It has been evaluated that, in respect to a hybrid engine, a liquid engine is a valid but not the best choice for the SALTO I vehicle. The liquid bipropellant mixtures which satisfy our requirement nowadays are LH_2/LO_2 and LCH_4/LO_2, but due to the cryogenic property, these mixtures would require a very high cost of maintenance to guarantee such performance. The final choice fell instead on the use of a Hybrid Engine System, because it guarantees to have adequate performance for the mission with considerable weight reduction of fuel. Moreover, conventional hybrid systems offer several important advantages over their liquid and solid counterparts that potentially make them attractive for different applications, such as:

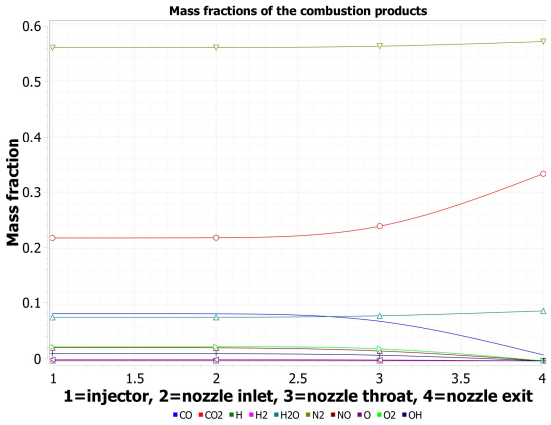

Figure 2- Mass fraction of comb products

- Safety: Hybrid rocket engine boost safety, compared to liquid and solid rocket engines, due to no explosive fuel combustion which permits a very low chance of failure in the system.
- Simplicity: in solid propellant both fuel and oxidizer are completely mixed, while on hybrid-fuel grains are insensitive to cracks and imperfections because they are inert. Moreover, cryogenic tanks are not required.
- Reliability: because only the oxidizer is stored in liquid form, hybrid rockets require only half as much feed-system hardware as liquid-propellant rockets.
- Environmental friendliness: in our case, using propellants such as Nitrous oxide (N_2O) and rubber-based fuel such as HTPB, it's possible to have environmentally clean combustion without, for instance, adding aluminum dust, which can be ecologically damaging.
- Low cost: Hybrid rockets pose almost no explosion hazard during manufacture, transport, ground test, and storage because the fuel and oxidizer are separated both physically and by phase.

3. Engine Parameters

Once choosing the propellant and the trajectory of the vehicle, the focus was on combustion chamber pressure, nozzle's area ratio and mixture ratio. These three parameters are not independent from each other, so an iterative analysis was done using MATLAB to compute the data provided by RPA.

3.1 Combustion Chamber Pressure

The combustion chamber pressure influences the total thrust provided by the rocket and varies during the mission. Once chosen for the fuel-oxidizer combination and the operational altitude range, the combustion pressure must be fixed in such a way that the rocket will provide the total thrust requested [310 kN] and to protect the combustion chamber itself to prevent structural damage. As shown in the Figure 3, the ratio between the combustion chamber pressure and the external pressure has to be chosen, since the external pressure varies from 0.193 atm at 12000 meters to 2.0e-5 atm at 75000 m. A pressure ratio ranges from 100 to 1000 was chosen. To run the analysis, a stoichiometric mixture ratio equal to 8.6 (according to RPA), a burn time of 85 s and an area

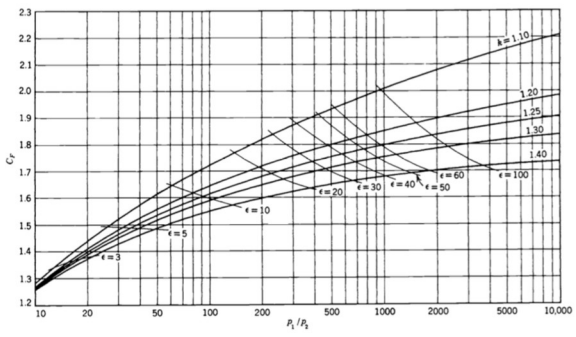

Figure 3 - Thrust coefficient to pressure ratio

ratio equal to 35, similar to the third stage of the Saturn V (that operated in a similar altitude range) have been chosen. Providing these inputs to RPA, together with the high-level requirements, the fuel-oxidize combination, and the operative altitude range of the mission, a pressure-variable analysis was conducted. It showed that a combustion chamber pressure of 34.5 bar is near to the minimum value that provides sufficient thrust to accomplish all the requirements [7]. It is relevant to notice that an in-depth structural and thermal analysis could show a higher permissible pressure, but here it was chosen to select the minimum acceptable value to remain conservative.

3.2 Nozzle's Area Ratio

To avoid separations, it is important to not let the exhausted gasses expand excessively through the nozzle. On the other hand, if they do not expand sufficiently, all the potential thrust that our nozzle could provide is not exploited. Since the altitude and the external pressure are not constant, a trade-off has to be done. The thrust coefficient evolution has been analyzed because it is related to the performances of the nozzle design. The Figure 4 shows that the optimal ε grows with the pressure ratio (and so with altitude at fixed chamber pressure), starting from 22 at 12000 m to over 200 at 75000m. The area ratio should not be too high for weight and aerodynamics reasons. Looking at the results obtained in RPA, the thrust coefficient seems to not grow significantly from an area ratio over 35 at high altitudes, so this value was chosen for our nozzle.

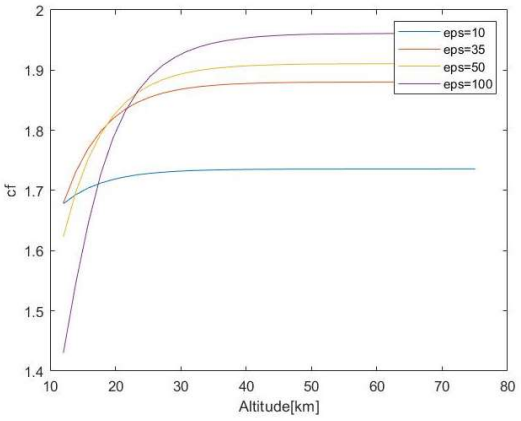

Figure 4 - Thrust coefficient evolution with altitude using ϵ as parameter

3.3 Mixture Ratio

The main parameters influenced by mixture ratio (MR) that will be discussed are rocket efficiency, mass of the propellant and pollution caused by the rocket.

3.3.1 Rocket Efficiency

Specific impulse I_{sp} and the thrust coefficient c_f are performance parameters that we want to maximize to achieve the required thrust using the minimum propellant mass. They vary with MR and in particular they have an optimal point. The Figure 5 obtained by RPA simulations shows that the maximal I_{sp} (in the vacuum) is reached approximately at MR=7.4 and remains roughly constant until MR=8.4. Thus, an arbitrary value of MR from 7.4 to 8.4 might be appropriated. The Figure 5 also shows the evolution of the thrust coefficient. Unfortunately, it has a maximum point at MR=8.6, so a trade-off was done. For this section, talking about efficiency of the rocket, an appropriate mixture ratio range will be approximately from 8 to 8.5.

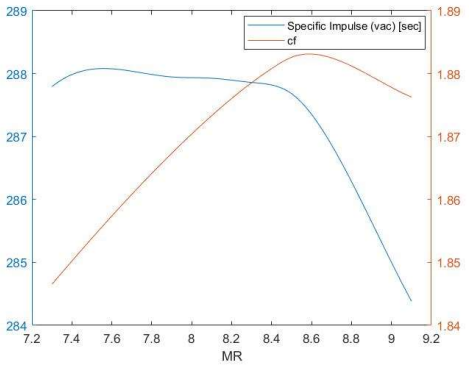

Figure 5 - Variation of vacuum specific impulse and thrust coefficient with MR

3.3.2 Fuel Mass

The fuel mass necessary to provide the thrust requested could be estimated by

$$M_{ox} = \dot{m}_{ox} \cdot t_{burn} \quad \text{and} \quad M_{fuel} = \frac{M_{ox}}{MR} \tag{1}$$

So the MR and the average oxidizer mass flux (which depends on the MR itself) have to be fixed. In particular, it was studied the value of the constant oxidizer flow necessary to obtain the required nominal thrust for each value of the mixture ratio. As expected, the oxidizer mass flux increases with the mixture ratio, but this evolution is nonlinear. It starts to increase more strongly after 8.4, thus that was the limit we chose not to exceed. In the same figure is reported the evolution of the specific impulse too, and it can be observed that 8.4 is the same

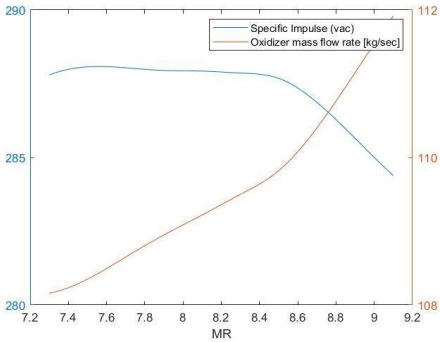

Figure 6 - Variation of specific impulse and oxidizer mass flow with MR

mixture ratio after which the efficiency starts to decrease. This fact confirms the limit chosen.

3.3.3 Pollution

Even if the propellant combination N_2O/HTPB is more environmentally friendly than commonly used options, it is possible to choose an opportune mixture ratio to decrease emissions even more. Because of the presence of nitrogen in the oxidizer, if the mixture ratio is too high, we inject a high quantity of N_2O, thus the risk to obtain NOx in the exhausted gasses grows. It is shown in the figure obtained by RPA, in which it can be seen that over MR=8.3 nitrous oxide quantitative is no more negligible. It has to be noticed that the graphic is on a semi-logarithmic scale.

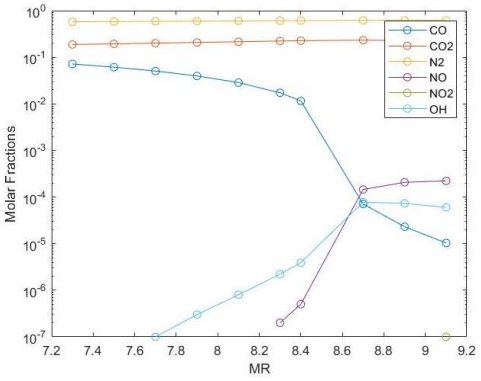

Figure 7 - Combustion products with MR variation

3.4 Conclusion

A MR=8.4 was chosen by making a trade-off that avails the engine to provide the requested thrust without exceeding the propellant mass and volume, and that reduces the NOx emissions with respect to the stoichiometric mixture ratio. The Table 1 summarize performances. It is now possible to estimate the total impulse provided by the engine using the definition:

$$I_{tot} = \int_0^{t_b} T dt \qquad (2)$$

An average value can be obtained considering the nominal thrust and multiplying it with the burn time:

$$\mathrm{I_{tot,av}} = T_n t_b = 310[kN] \cdot 85[sec] = 26350\ kNs \qquad (3)$$

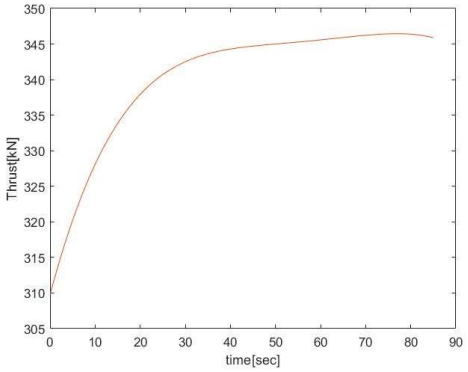

Figure 8 - Thrust variation with time

An actual estimation of the total impulse could be calculated by integrating numerically the data provided by RPA. As it is shown in the Figure 8, the actual thrust grows with the altitude and so the time. It is due to the lower atmospheric resistance present from 12 km to 75 km than at sea level, where the thrust is tested and respect to the nominal parameters are given. In conclusion, a greater actual total impulse provided by the rocket engine $I_{tot} = 28928\ kNs$ is obtained. This value will decrease due to the throttling choice that will be discussed later. A $I_{tot} > 26000\ kNs$ was estimated.

Parameters	Value	Unit of measure
Chamber thrust (vac)	346.31747	kN
Specific impulse (vac)	287.79916	s
Chamber thrust (opt)	328.60403	kN
Specific impulse (opt)	273.07881	s
Total mass flow rate	122.70555	$\frac{kg}{s}$
Oxidizer mass flow rate	109.65177	$\frac{kg}{s}$
Fuel mass flow rate	13.05378	$\frac{kg}{s}$
Oxidizer mass	9320.4	kg
Fuel mass	1109.57	kg

Parameter	Sea level	Vacuum	Unit
Effective exhaust velocity	1697.5200	2822.35	$\frac{m}{s}$
Specific impulse (by weight)	173.1	287.8	s
Thrust coefficient	1.1312	1.8808	

Table 1 – Delivered performances

4. N2O Tank

Regarding the rocket motor, there is a tank containing the liquid oxidant and the solid fuel is stored directly in the combustion chamber. The choice of architecture and materials to be used is fundamental in the design of the propulsion system, as they will influence both the performance, the stability and safety of the entire aircraft. The decision to use Nitrous oxide as an oxidant allows to exploit its self-pressurizing properties: in fact, thanks to its high vapor pressure of 5.0353 MPa at 293 K, it behaves like a saturated liquid, making it unnecessary to use turbopumps or other pressurization systems to inject N_2O into the combustion chamber, thus reducing the weight, complexity, and costs.

To study the behavior of the oxidant in the tank, it was assumed a fluid that is in equilibrium and follows the perfect gas law [3].

4.1 Design, Materials and valve choice

For the success of the mission, 9320.4 kg of liquid N_2O are needed; assuming that the liquid fraction is 95% of the total weight of the fluid, the total mass is 9810.9 kg. Since the density of liquid Nitrous oxide at 290 K and 4.8 MPa is 809.81 kg/m^3, it is easy to derive the volume occupied by the liquid by the formula $V = m/\rho$, where: V volume of the fluid; m mass of the fluid; ρ density of the fluid. The value of the volume of our oxidant tank will therefore be 12.115 m^3. These particular temperature and pressure values were considered because, under these conditions, the fluid remains completely liquid, the pressure is above the vapour pressure value, which is very useful in ground storage and tank refill conditions. The operating conditions of the aircraft are different, the pressure has to be below the vapour pressure in order to exploit the self-pressurizing properties of the liquid N_2O. It is simply necessary to raise the temperature of the tank and therefore of the fluid to 293 K, a temperature which corresponds to a higher vapour pressure value.

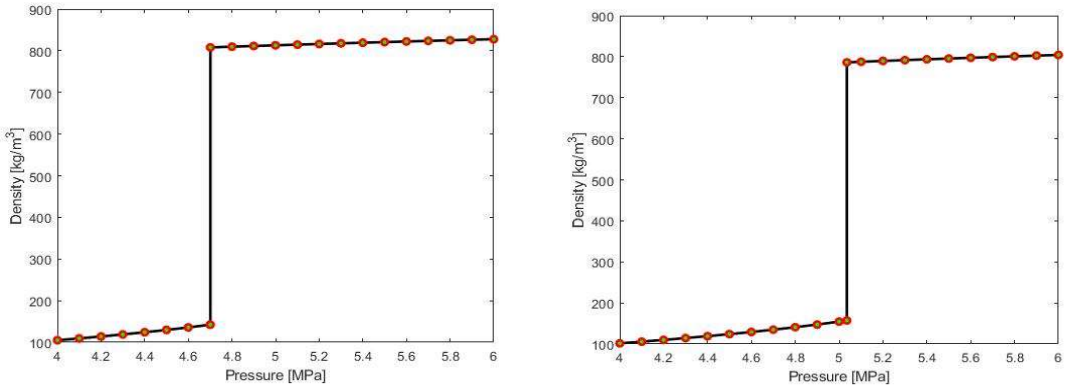

Figure 9 - Density on pressure variation [23]

The material to be used for the construction of the tank structure is aluminium, since it and its alloys have excellent mechanical characteristics that fall within our range of use. It is a material that, for the same performance, has a lower weight and density than other metals, it is easily machined and it is a very cheap and easily available metal. In particular, the aluminium alloy we rely on is EN AW-6082 T6. Furthermore, to the choice of the valve of N_2O tank that conducts to the combustion chamber, after a research in literature, the use of "ball valves" has been chosen for the very high flow coefficient, inexpensive and low drop pressure property. In order to guarantee a cheap option and a very low drop of pressure, we select this one, with material covered by Teflon, to operate on the main pipe of the oxidizer tank.

4.2 Throttling

Although hybrid engines are undoubtedly interesting in terms of cost, simplicity and affordability, they have some trivial issues on throttling systems. Hybrid motors, since they use a solid fuel and a liquid oxidizer, are a little less precise when it comes to throttling. In fact, it's possible to manage only the oxidizer flow, and the fuel flow is a function of it. Moreover, a hybrid engine changes the amount of MR over time, based on the transformation of the combustion chamber. The radius of the ports in the chamber continues to increase, and the fuel mass flow decreases. One big problem occurs when the thrust of a hybrid engine decreases, because a variation of MR will occur. If we explicit oxidizer and fuel mass flow, we can observe that both are proportional to the oxidizer mass flux, but by a different exponent:

$$\dot{m}_{ox} = G_{ox}A_p = G_{ox}R^2\boldsymbol{\pi} \propto G_{ox} \quad (4)$$

$$\dot{m}_f = \rho_b A_b a {G_{ox}}^n \propto {G_{ox}}^n \quad (5)$$

Based on such differences, we can use the AOIM system [9] to redirect part of the oxidizer flow on the aft part of the combustion chamber, and the residual part, to maintain the same value of MR, must be directed axially into it. The values are figured in Table 2, which study has been assessed to maintain the same MR on throttling variation.

Parameters	80%Throttling	60%Throttling	40%Throttling
Thrust	263.2921	197.4691	131.6461;
$\dot{m}_{tot}$	98.3171	73.7378	49.1586;
$\dot{m}_{ox}[Axial]$	80.204	53.484	30.214;
$\%\dot{m}_{ox}[AFT]$	6.97%	11.3%	12.49%;

Table 2 - Percentage of oxidizer mass flow that must be injected on the aft part of the combustion

5. Combustion Chamber

5.1 Sizing of combustion chamber and grain design

Classical hybrid rocket engines show a variety of advantage and disadvantage, such as:

- Slow regression rate compared to a solid rocket engine.
- Thrust variation on burn time.
- Fuel residuals, which not all the fuel burns.
- Mixture ratio changes on burn time.

In order to study the regression rate of a hybrid rocket, it is necessary to conduct experimental and practical processes to evaluate such performance but, in first analysis, it is still possible to analyze the regression rate of the grain thanks to empirical and general techniques. Considering the general formula of the regression rate:

$$r = aGo^n x^m = \frac{dR}{dt} = a\left(\frac{\dot{m}_{ox}}{NR^2\boldsymbol{\pi}}\right)^n x^m \quad (6)$$

Supposing a 1-Dimensional study of the combustion process on time variation, the grain structure and design of the engine could be studied. It has been considered a 'n' of 0.71 (length coefficient) [5] from iterations. A exponent 'm' (oxidizer mass flux coefficient) = 0 as ideal model [6] and a hybrid mixture coefficient $a = 0.198$e-4 as the general value of HTPB/N_2O mixture [6].
The length and diameter limit for sizing both N_2O tank and HTPB chamber are very limited, with length and diameter maximum of 6.481m and 1.843m. For both, a threshold of 20% has been considered for structure limitation, reducing respectively to 5.184m in length and 1.513m in diameter. By the regression rate formula (6), it is now possible to determine the radius of every grain for the three structures proposed. Integrating the formula (6) from an initial and final radius, it is now possible to calculate different sizes for the three types of configuration described below.

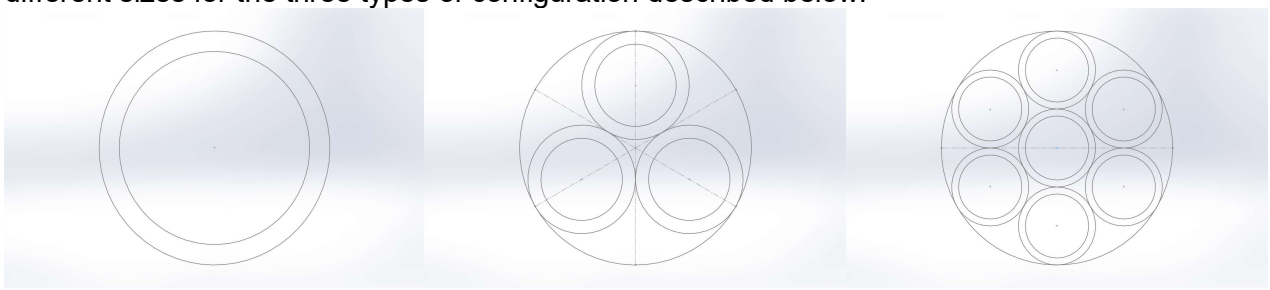

Figure 10 - Single, three and seven ports structures

Parameter	1 Holes	3 Holes	7 Holes
Ri	0.6565 [m]	0.2661 [m]	0.2022 [m]
G_o	81.1094 $[\frac{kg}{m^2 s}]$	164.5682 $[\frac{kg}{m^2 s}]$	122.1866 $[\frac{kg}{m^2 s}]$
$\dot{r}$	0.4885 $[\frac{mm}{s}]$	0.74177 $[\frac{mm}{s}]$	0.60042 $[\frac{mm}{s}]$
L	8.7178 [m]	4.3383 [m]	3.0233 [m]
Filling	24.69 %	62.8827%	50.0081 %
Residual	18.32%	56.2669%	44.4372 %

Table 3 – Data taken from given analysis

Describing Table 3, for one single port with circular diameter, different positive aspects can be seen, which low filling and residual (obviously a reduction of these parameters gives cheap and affordable benefits), but a chamber length of 8.7178 m must be changed, because dimension of our suborbital vehicle doesn't match, which smaller than our theoretical space. A three port grain structure could be the most problematic, not only because of the very limited use of the grain (with a value of filling and residual very high), but also in terms of weight. A high regression rate has been demonstrated, but the disadvantage could be drastic. A seven port grain is the most complex architecture. The filling and residual value are on average, but the benefits are huge: the length of the chamber is very short and it adapts to the needs.

In conclusion, the seven-port structure has been chosen for the combustion chamber.

5.2 Preliminary evaluation about 1D analysis on chamber length

Although the assessment for the seven-hole structure has been verified, it should be mentioned that in a real combustion chamber, the fuel is immersed in a turbulent boundary layer, with the positioning of the flame in such a boundary and with heat transfer. All these aspects have been avoided to an ideal and simplified preliminary evaluation, but in a real case, issues are different. In fact, for instance, in function of the chamber length, the regression rate is determined with time and space [4], as illustrated. The solution selected to this phenomena is simple: making the fuel grain thicker and decreasing the inner radius of every grain fuel, which was initially considered, by 20%, as shown in Table 3.

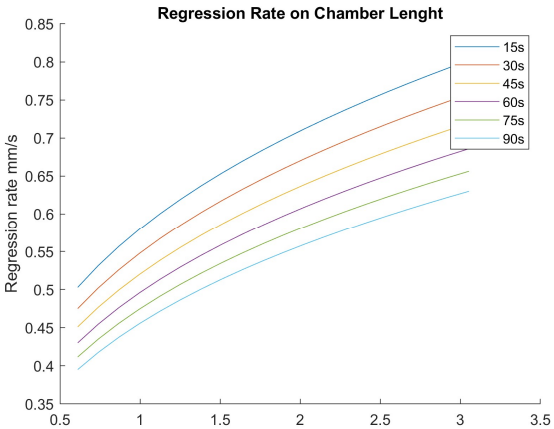

Figure 11 - Consequences through the combustion chamber length

5.3 Injector

For the oxidizer injector, we have chosen one respecting the characteristics of efficiency and stable combustion, in which a homogeneous injection with atomized droplets is needed. After a literature analysis [14], 45°-inclined injectors is the most stable during rocket engine hot runs of the N_2O oxidizer and lead the right atomization level needed.

5.4 Swirl Option

The swirl effect is a particular condition which oxidizer from the tank of N_2O can be injected, permitting the oxidizer to flow on the chamber with a swirl effect. This phenomenon can generate a variation of the fuel regression rate [2]. The basic idea is that the mixture ratio shift can be compensated by acting in real time on the coefficient "a" of the fuel regression rate. If the injection swirl number can be changed on demand, the regression rate can be adjusted to balance the oxidizer flow in order to contrast a strong lack of oxidizer flow and thus maintain a constant mixture ratio on time and for single port grain, improve specifics and reduce drastically the size of the length chamber. Supposing a single-port structure, and avoiding a solution to the seven-port structure considering the complexity of the grain, we can utilize the configuration called A-SOFT [22]. The fuel regression rate in the A-SOFT configuration is described by the following equation (S_g = Geometric swirl; S_e= Effective swirl):

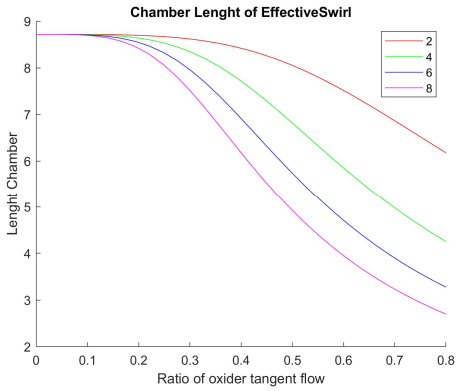

Figure 12 - Length of the chamber on oxidizer tangent flow ratio

$$r = a(1 + Se^2)Go^n x^m \rightarrow Se = \frac{Sg}{(1+\frac{\dot{m}_{oAX}}{\dot{m}_{oTG}})^2} \quad (7)$$

In order to see the high consequences in our engine, adding more than 6 to 8 pipes in order to inject the oxidizer in such a way, we can decrease the chamber length up to 3 meters. The added complexity of the feed system brings us to evaluate this option, but to discard it and remain for a complex grain structure, but easier to handle than this solution.

5.5 Materials

When it came to choosing the materials to be used for the structure of the combustion chamber of the rocket motor, the high temperatures reached during combustion severely limited the range of possible choices. There are two main hypotheses being considered: using filament winding technology for the structure of the combustion chamber but losing the possibility of reuse [11]; using metal superalloys with high resistance to extreme temperatures, further coated on the inner wall with a layer of ablative materials, raising manufacturing and especially maintenance costs, but maintaining the possibility of reuse. The latter solution was chosen because it has a lower environmental impact and makes the whole propulsion system reusable. The alloy most suitable for our purpose is Inconel 625, a nickel-based superalloy that possesses high strength properties and resistance to elevated temperatures. It

also demonstrates remarkable protection against corrosion and oxidation. As an ablative material, zirconium diboride is an interesting solution; it is an ultra-refractory ceramic material with a melting point of 3519 K. The use of this ceramic material instead of the lighter graphite, allows better resistance to the higher temperatures typical of the combustion chamber. The use of these two materials therefore allows the tank to be reused, but significantly increases its weight.

6. Nozzle Design and Thermal Analysis

The nozzle is subjected to high temperatures that should be analyzed to choose the more appropriate material and, if it will be necessary, a refrigeration system. Thus, before exploring these two aspects, a possible range of temperatures in which the nozzle, especially the throat area, will work and the heat flux exchanged has to be estimated. To do so, the empirical formula of Bartz was applied for a 0D analysis, providing the boundary condition by a 1D analysis in RPA and a 2D analysis of the temperature profile through the nozzle in ANSYS.

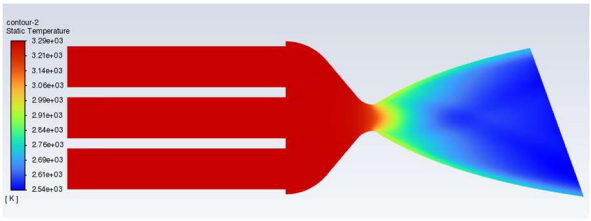

Figure 13 - Evolution of the static temperature on chamber and nozzle engine

6.1 Design and Validation

The bell shape was designed by implementing the method of characteristics in MATLAB. To determine the shape of the junction between the combustion chamber and the nozzle's throat, and the throat itself, the geometric nominal data of the third stage of Saturn V was chosen as the first attempt. Then a 2D simulation in ANSYS was conducted, providing the RPA outputs as boundary conditions. The final design parameters were obtained by an iterative analysis in order to not generate separation, especially in the throat section. The θ_{cut} choice will be discussed later.

Parameters	Value
R_2	534.82 mm
R_n	49.97 mm
θ cut	70°
b	45°
T_n	34°
T_e	10.5

Table 4 - design of combustion chamber and nozzle

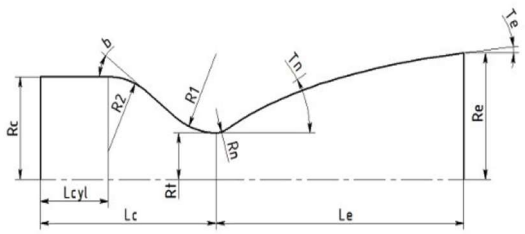

Figure 14 - Schematic representation of the nozzle's design parameter

6.2 Thermal Analysis and Cooling

The Bartz formula [17] is used in thermodynamics to calculate the convective heat transfer coefficient. This method consists in solving a system of three equations. Since the solution depends on the Mach of the exhausted gasses, a nozzle's section has to be fixed to run the analysis. In the throat section, where M=1, the heavier thermal load is reached, so the analysis was conducted for the throat and for the bell separately.

6.2.1 Throat Analysis

The convective heat transfer coefficient resulting by solving the Bartz equation is $h_g = 15.5579 \frac{kW}{m^2 K}$. To estimate the heat flux was used the electrical equivalent of the power, threatening the coefficient h_g as a resistance and the heat flux as a current flux:

$$q = h_g(T_{aw} - T_{wg}) \tag{8}$$

where $T_{aw}$is the adiabatic wall temperature. A heat flux $q = 11.9687 \frac{MW}{m^2}$ and a $T_{wg} = 2382.6\ K$ were obtained. As expected, the temperature in the throat is too high. A removable carbon insert [18] [10] in the throat is a possible solution discussed here. It will protect the nozzle during the burning phase, but its erosion will probably make it not reusable, so it shall be substituted after every launch. Without this component, the nozzle will not result reusable, so this seems to be a valid trade-off. To estimate the new critical temperature a similar analysis was conducted, but a new convective heat transfer coefficient had to be defined, the one relative to the heat exchange between the carbon film and the gasses

$$h_{gc} = \frac{1}{\frac{1}{h_g} + R_d} \tag{9}$$

where $R_d = 0.373 \frac{m^2}{MW}$ is the thermal resistance of the carbon insert [19]. The new throat wall temperature was obtained by:

$$T_{wg} = \frac{\frac{T_{wc}}{R_d} - h_g T_{aw}}{\frac{1}{R_d} - h_{gc}} \tag{10}$$

where T_{wc} is the temperature in the layer that separates the carbon insert and the gasses. A new temperature of $T_{wg} = 615.6695\ K$ was obtained. This lower value allows us to choose between a large range of possible materials since even aluminium is able to tolerate it [12].

6.2.2 Bell Analysis

The same analysis was conducted for several sections of the bell. The heat flux evolution through the bell obtained is shown in the Figure 15. As predictable, the heat and the average wall temperature $T_{wg} = 2211.1\ K$ are lower in the bell, so we could use an alternative method to refrigerate this zone, saving weight, costs and reducing the operational complexity. The bell could be cooled in a radiative way. To investigate the feasibility of this method the heat flux calculated by the Steffan-Boltzmann was equalized to the one calculated with the electrical equivalence:

$$q = B\epsilon {T_{wg}}^4 = h_g(T_{aw} - T_{wg}) \tag{11}$$

where B is the Stefan-Boltzmann constant and ϵ is the hemispherical emissivity of the material. The temperature reached by using radiation cooling results:

$$T_{wg} = \sqrt[4]{\frac{h_g}{B\epsilon}(T_{aw} - T_{wg})} \tag{12}$$

that is nonlinear and has to be solved in a numerical way. The temperature evolution through the nozzle by using radiative cooling is shown in the Figure 16, where ϵ is used as a parameter.

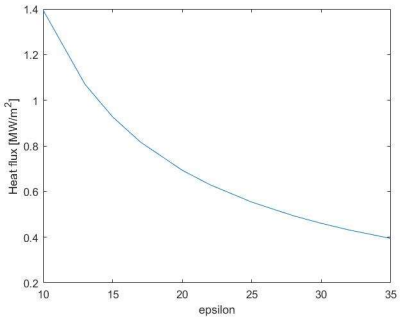

Figure 15 - Heat transfer through the nozzle bell

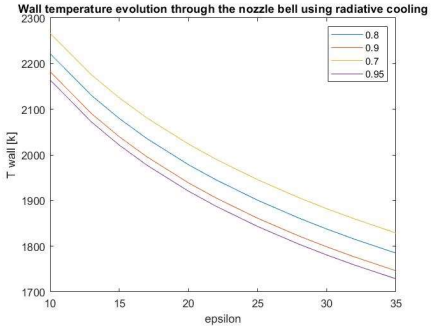

Figure 16 - Evolution of the static temperature through the nozzle bell using emissiity as parameter

7. Thrust Vectoring Control

Once fixed the engine's parameters and thus the total impulse provided by the rocket, it is essential to define how this thrust will be directed. A simplified analysis to support the choice of the cut nozzle is presented. This interesting solution was applied in the RocketMotorTwo and in the engine here studied can be a valid support to the main thrust vectoring control adopted, which could be the frictionless flex-gimbal mechanism with limited angle torque motor presented by Almatech [21] or others more common solutions. It can be the main TVC itself if used along with the throttle.

7.1 Cut Nozzle

During the rocket phase, the vehicle curves from a near-horizontal asset to a near-vertical one, thus the rocket engine will not provide an axial thrust, but it has to make the trajectory curves to reach the ballistic phase. A nozzle that on design tends to deviate the gasses to obtain a non-axial thrust could result in less structural stresses and complexity than other TVC systems. Strong simplifications were made to analyze the effect of the cutting. All the pitch angle variation was assumed to be provided by the cut in the nozzle exit area section by deviating the exhausted gasses. Moreover, the total thrust vector has been considered perpendicular to the nozzle exit area and applied in the nozzle exit area. Naming L_{ba} the instantaneous distance between the nozzle exit area and the barycentre, the bending

momentum will be

$$M = F_N \cdot L_{ab} \text{ where } F_N = F_{nominal} \cdot sin(90 - \theta) \quad (13)$$

By approximating the vehicle to a rigid beam for the inertia estimation:

$$I\alpha = m_{tot} r^2 \alpha = F_{nominal} \cdot sin(90° - \theta) \cdot L_{ba} \quad (14)$$

where m_{tot} is the total mass of the vehicle, r is his total length and α is the angular velocity. The cutting angle simplified formula resulting is:

$$\theta = 90° - arcsin(\frac{m_{tot} r^2 \alpha}{L_{ba} F_{nominal}}) \quad (15)$$

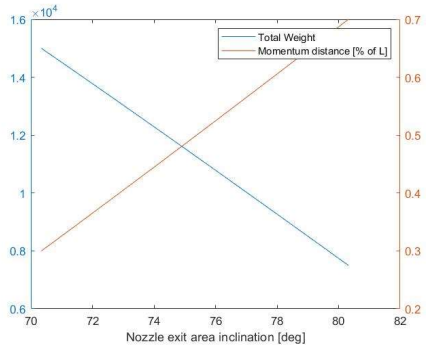

Figure 15 – Optimal θ for each total mass and L_{ab}

This equation shows that the more the vehicle is heavy, the higher will be the cutting angle and that θ is not constant during the burning phase, as well as the thrust provided by the engine. Another parameter that is not constant during the burning phase is L_{ba}. It demonstrates that for every instant of the combustion an optimal cutting angle can be defined. Since the propellant is expelled, the barycentre will move forward, even if there is of course a limit due to stability issues. In conclusion, this analysis suggests that a lower cutting angle will provide more assistance to the main thrust vectoring control system, so for our design, we fixed $\theta = 70°$. In a real situation, an angle that doesn't make the flux separate should be chosen. Structural failures and damages have to be considered as well.

8. Air Breathing Engine and Feed System

Initially, trying to always operate in the green field, the propfan was considered. The propfan is a modified turbofan in which the fan is located outside the engine case. The propfan engine is part of the engines with a large dilution ratio and its use allows it to operate with almost 30% less fuel consumption. However, it must be considered that the engines currently on the market do not guarantee the resistance of the blades to supersonic conditions reached during the mission when the rocket motor is turned on, compromising the structural stability and therefore not guaranteeing the success of the mission in the re-entry phase.

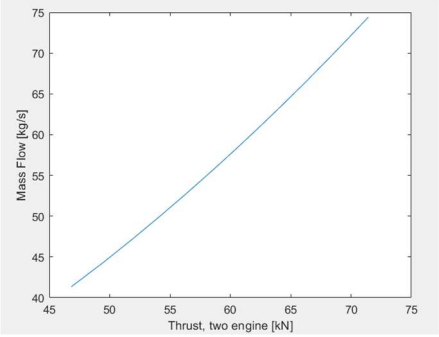

Figure 16 - Trend of the mass flow as the thrust varies

For the reasons explained above a turbofan of Pratt&Whitney competence was considered, in particular the use of two PW308 engines allows it to reach the necessary thrust in total safety. This engine provides a take-off thrust of 31.15 kN with a high by-pass ratio. It is characterized by an external diameter of 1.299 meters and a length of 2.184 meters. The total dry weight is 625 Kg, but it was estimate a total mass of 700 kg, one engine, including feeding system.

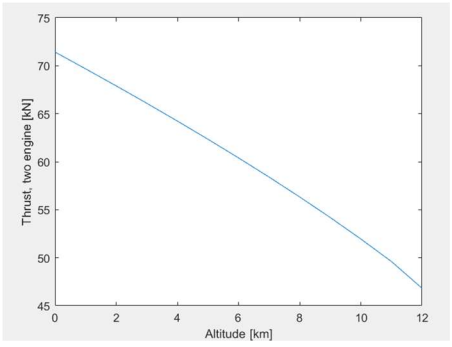

Figure 17 - Trend of thrust as the altitude varies

Taking into consideration the mission profile designed for this aircraft [20], the performance trend with altitude is shown in the Figure 21. The results obtained in this analysis are consistent for this kind of engine. Two engines are therefore sufficient to be able to support the aircraft in its mission phases.

8.1 Feed System

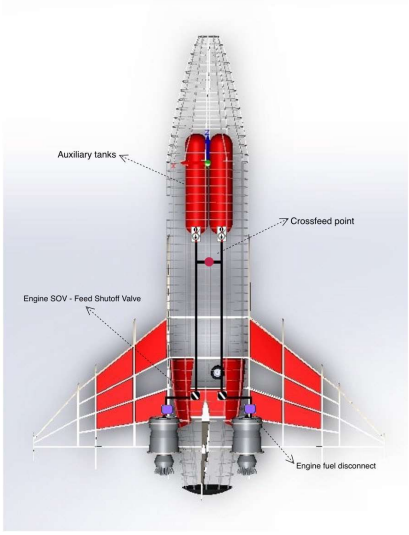

Figure 18 - Auxiliary feed sys-

The purpose of the fuel installation is to stow the necessary fuel and bring it to the thrusters under the necessary pressure and flow conditions. The system is designed to withstand failure and maintain proper engine operation. In larger aircraft the tank is a complex problem solution because of its remarkable volume. This volume is usually divided into several parts to facilitate installation on board. The location of the tanks is generally inside the wing boxes, for the unused space inside them but also to better distribute the weight of the fuel. When multi-engine airplanes are used, it shall be possible to power any engine with the fuel of any tank. The scheme of the feed system is based on Boeing 727, as it also has the engines in the tail and not arranged along the wings. The feed system is divided into auxiliary and main, where the two main valve types are the engine fuel disconnect and the engine feed shutoff valve, because fuel is piped through fuel lines to a fuel control valve. These valves are required to prevent fuel reaching the engine in case of an engine fire. In the case of airplanes multi-engine is provided for the possibility of feeding crossed (crossfeed), must therefore be possible from any tank reach any propeller and, at the same time, nourishing simultaneously two thrusters. In the case of cross-feeding, account must be taken of the fact that the request to the pump in emergency conditions can reach twice that required under normal operating conditions. If the crossfeed is close to the pumps even in these conditions the flow in the pipes remains practically equal to normal operation and consequently the loss of load. On the contrary with a crossfeed line away from the tanks and close to the engines the flow in pipes in emergency would be double and therefore the pressure drops four times those in normal operation. For this reason, we decided to place our crossfeed point as far away from the engines as possible, in this way we also avoid additional weight at the rear of the airplane where the tanks of the main fuel system and the weight of the engines are already present. In this way, in case of problems with the main tanks you can isolate the damaged tank and make the auxiliary circuit become the main one.

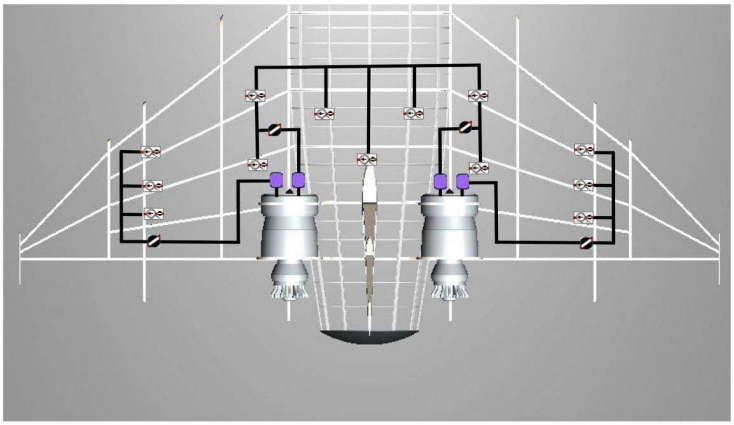

Figure 19 - Main feed system

9. Conclusion

Our objective was to realize the entire propulsion system for the vehicle SALTO I.
The propulsion system, achieved by modifying the existing SALTO I project switching from a liquid system to a hybrid one, compliant all the high level requirements imposed by the Challenge and reduced the engine's weight. After this preliminary analysis, it results to be reusable in almost all its components apart from the removable carbon insert in the nozzle throat and the layer of zirconium diboride in the combustion chamber. These exceptions were adopted to save and make reusable all the thrust chamber instead of replacing it every launch or using different cooling systems which could make our vehicle heavier and more complex.
We would like to point out that the N_2O/HTPB propeller is stable and green itself, but also our design decisions were taken to reduce environmental impact even more, such as mixture ratio choice and considerations made on grain additives.

Figure 20 - An overview of the hybrid engine

10. Contact Author Email Address

The contact author email address is : s281857@studenti.polito.it or brunomartina@hotmail.it .

11. Copyright Statement

References

[1] Federal Aviation Administration. "*Final environmental assessment for the launch and reentry of SpaceShipTwo reusable suborbital rockets at the mojave air and space port*". In: (2012).
[2] Barato Francesco , Toson Elena , and Pavarin Daniele . "*Variations and control of thrust and mixture ratio in hybrid rocket motors*". In: Advances in Astronautics Science and Technology 4.1 (2021), pp. 55–76.
[3] Borgdorff Steven . "*Nitrous oxide state estimation in hybrid rocket oxidizer tanks*". In: (2017).
[4] Grefen Benedict et al. "*Design, production and evaluation of 3D-printed mold geometries for a hybrid rocket engine*". In: Aerospace 8.8 (2021), p. 220.
[5] Karabeyoglu M Arif , Cantwell Brian J , and Zilliac Greg. "*Development of scalable space-time averaged regression rate expressions for hybrid rockets*". In: Journal of Propulsion and Power 23.4 (2007), pp. 737–747.
[6] Kuo Kenneth K and Chiaverini Martin J. *"Fundamentals of hybrid rocket combustion and propulsion". American Institute of Aeronautics and Astronautics.* In: (2007).
[7] Masseni Filippo . "*Optimization approaches under uncertainty for hybrid rocket engines*". In: (2020).
[8] Nosseir Ahmed ES, Cervone Angelo, and Pasini Angelo . "*Review of state-of-the-art green monopropellants: for propulsion systems analysts and designers*". In: Aerospace 8.1 (2021).
[9] Ozawa Kohei and ShimadaToru . "*A theoretical study on throttle ranges of O/F controllable hybrid rocket propulsion systems*". In: Journal of Fluid Science and Technology 13.4 (2018), JFST0031–JFST0031.
[10] Poulopoulos John and Chronopoulos Theodoros . "*Cooling methods in combustion chambers and nozzles*". In: (2020).
[11] Quanjin Ma et al. "*Filament winding technique: SWOT analysis and applied favorable factors*". In: SCIREA Journal of Mechanical Engineering (2019).
[12] Reed Brian D , Biaglow James A , and Schneider Steven J . "*Iridium-coated rhenium radiation-cooled rockets*". In: International Symposium on Rhenium and Rhenium Alloys. NASA-TM-107453. 1997.
[13] Sutton George P and Biblarz Oscar. "*Rocket propulsion elements*". John Wiley & Sons, 2016.
[14] Waxman Benjamin S. "*An investigation of injectors for use with high vapor pressure propellants with application to hybrid rockets*". In: (2014).
[15] Student Aerospace Challenge, "*General characteristic of vehicles*". In: (2021).
[16] Bergamini Sibilla et al. *"SALTO Suborbital Analysis of a Lightweight spaceplane"*. In: (2021).
[17] Iqbal, M. J., et al. *"Comparison of empirical correlations for the estimation of conjugate heat transfer in a thrust chamber."* Life Science Journal 9.4 (2012): 708-716.
[18] KAMPS, Landon Thomas. "*Mechanisms of graphite nozzle erosion in hybrid rockets*". In: (2019).
[19] Silva, Homero Paula and Pardini. "*Shear properties of carbon fiber/phenolic resin composites heat treated at high temperatures*". In: (2016).
[20] Za Alberto et al. "*Project Catfish Structure suited for suborbital flight Défi Aérospatial Etudiant Subsystems integration and safety analysis*". In: (2020)
[21] Dr Fabrice Rottmeier Anett Krammer et al. *"Novel Thrust Vectoring Mechanism"*. In: (2019).
[22] Usuki T, Shimada T (2015) *"Improvement on thrust profile flexibility by oxidizer-to-fuel ratio feedback control in hybrid rockets"*. In: Proceedings of the 66th International Astronautical Congress (IAC), Jerusalem, Israel, 12–16 October (2015).
[23] *"Thermophysical Properties of Fluid Systems"*. In: (2022). url: https://webbook.nist.gov/chemistry/fluid/